China Geology 4 (2021) 658−672

China Geology

Journal homepage: http://chinageology.cgs.cn
https://www.sciencedirect.com/journal/china-geology

Age and geochemistry of the granitoid from the Lunte area, Northeastern Zambia: Implications for magmatism of the Columbia supercontinent

Hong-wei Sun[a, b], Jun-ping Ren[b,*], Jie Wang[b], A-lei Gu[b], Xing-yuan Wu[b], Fu-qing He[b], Li-bo Zuo[b], Chipilauka Mukofu[c], Alphet Phaskani Dokowe[c], Ezekiah Chikambwe[c], Zi-jiang Liu[d], Shi Xing[d]

[a] *School of Earth Science and Resources, China University of Geosciences (Beijing), Beijing* 100083, *China*
[b] *Tianjin Center, China Geological Survey, Tianjin* 300170, *China*
[c] *Geological Survey Department of Zambia, Lusaka P.O. Box.*50135, *Zambia*
[d] *No.* 5 *Geological Brigade, Hebei Bureau of Geology and Mineral Resources Exploration, Tangshan* 063000, *China*

ARTICLE INFO

Article history:
Received 8 May 2021
Received in revised form 12 September 2021
Accepted 2 November 2021
Available online 15 November 2021

Keywords:
Paleoproterozoic
S-type granite
Bangweulu Block
Geological survey engineering
Lunte area
Northeastern Zambia

ABSTRACT

The Paleoproterozoic tectonic evolution of the Bangweulu Block has long been controversial. Paleoproterozoic granites consisting of the basement complex of the Bangweulu Block are widely exposed in northeastern Zambia, and they are the critical media for studying the tectonic evolution of the Bangweulu Block. This study systematically investigated the petrography, zircon U-Pb chronology, and petrogeochemistry of the granitoid extensively exposed in the Lunte area, northeastern Zambia. The results show that the granitoid in the area formed during 2051±13–2009±20 Ma as a result of Paleoproterozoic magmatic events. Geochemical data show that the granites in the area mainly include syenogranites and monzogranites of high-K calc-alkaline series and are characterized by high SiO_2 content (72.68% – 73.78%) and K_2O/Na_2O ratio (1.82–2.29). The presence of garnets, the high aluminum saturation index (A/CNK is 1.13–1.21), and the 1.27%–1.95% of corundum molecules jointly indicate that granites in the Lunte area are S-type granites. Rare earth elements in all samples show a rightward inclination and noticeably negative Eu-anomalies (δEu = 0.16–0.40) and are relatively rich in light rare earth elements. Furthermore, the granites are rich in large ion lithophile elements such as Rb, Th, U, and K and are depleted in Ba, Sr, and high field strength elements such as Ta and Nb. In addition, they bear low contents of Cr (6.31×10^{-6}–10.8×10^{-6}), Ni (2.87×10^{-6}–4.76×10^{-6}), and Co (2.62×10^{-6}–3.96×10^{-6}). These data lead to the conclusion that the source rocks are meta-sedimentary rocks. Combining the above results and the study of regional tectonic evolution, the authors suggest that granitoid in the Lunte area were formed in a tectonic environment corresponding to the collision between the Tanzania Craton and the Bangweulu Block. The magmatic activities in this period may be related to the assembly of the Columbia supercontinent.

1. Introduction

The geodynamic evolution of the Bangweulu Block in northeastern Zambia is typically attributed to the influence of the Paleoproterozoic Ubendian Orogeny, the Mesoproterozoic Kibaran or Irumide Orogeny, and the Neoproterozoic Lufilian Orogeny. Its unique geographical location allows for better recording information about the magmatic, tectonic, and metamorphic activities related to the above-mentioned orogenic events, which is of great significance for the study of the regional tectonic evolution in Central Africa (De Waele B et al., 2006a, 2006b, 2008; Debruyne D et al., 2014; Kazimoto EO et al. 2015; Ren JP et al., 2017a). Previous studies have shown that the Bangweulu Block is mainly composed of basement complex and sedimentary cover (Brewer MS et al., 1979; De Waele B et al., 2005; Ren JP et al., 2016, 2020, 2021a, 2021b). The basement of the block is mainly composed of many Paleoproterozoic granitic rocks. However, its accurate formation age, as well as whether Archean remnants exist in it, is yet to be ascertained. The early understanding of its basement age was obtained from the age data of detrital zircons in the granitic and volcanic rocks near

First author: *E-mail address*: shwcub@163.com (Hong-wei Sun).
* Corresponding author: *E-mail address*: rjp2333@126.com (Jun-ping Ren).

Literary editor: Li-qiong Jia
doi:10.31035/cg2021048
2096-5192/© 2021 China Geology Editorial Office.

Mansa in the southwest (Brewer MS et al., 1979; Saviaro K, 1979; Schandelmeier H, 1980), the southern edge and the contact zones of the Irumide Belt (De Waele B et al., 2005, 2006a, 2006b; Debruyne D et al., 2014; Ren JP et al., 2018a, 2018b) and the Lufilian Belt (Rainaud CL et al., 2002; Master S et al., 2005; Armstrong RA et al., 2005; Ren JP et al., 2013), from which it was inferred that its basement was formed during 1800 –2060 Ma. In recent years, some researchers have successively obtained zircon U-Pb ages of 2012–1913 Ma (Ren JP et al., 2019a, 2019b, 2019c; Gu AL et al., 2020, 2021) in the eastern Kasama area and the Kapatu area. In addition to the formation ages, the Paleoproterozoic tectonic evolution of the Bangweulu Block has also long been controversial. There are two main points of view: (1) Brewer MS et al. (1979) and Kabengele M et al. (1991) suggested that the 1850 Ma high K calc-alkaline felsic igneous rocks in the Bangweulu Block represent an active continental margin arc environment related to the Ubendian Belt. This is similar to the view of Andersen LS and Unrug R (1984) that the metamorphic volcanic rocks related to the high K calc-alkaline series exposed in the northwestern part of the Bangweulu Block were formed in a subduction system. (2) Kazimoto EO et al. (2015) believed that the Bangweulu Block was in a passive continental margin environment in the early stage of the Ubendian orogeny (2640–1840 Ma). Therefore, it is necessary to further study the basement granites of the Banwewulu Block to provide new constraints for the regional tectonic evolution of central Africa during the Paleoproterozoic.

In recent years, the authors found a typical "dual structure" phenomenon consisting of basement complexes and sedimentary cover in the working area during the geological mapping in the Lunte area, northeastern Zambia. The basement complexes in the area account for approximately 90% of the working area and mainly include granitoid, providing favorable chances to study the tectonic-magmatic evolution of the Bangweulu Block during the Paleoproterozoic. This paper presents zircon U-Pb age data and major and trace element data of granitic plutons in the central part of the Bangweulu Block to explore the formation age, petrogenesis, magma source, and tectonic setting of the Bangweulu Block and, further, to assess the role of the Bangweulu Block in the assembly of the Columbia supercontinent.

2. Geological background

The Lunte area in northeastern Zambia is located in the central part of the Bangweulu Block (Figs.1a, b), which is named after the Bangweulu Lake and covers an area of approximately 150000 km^2. It is adjacent to the Congo-Tanzania Craton and is surrounded by a series of Paleoproterozoic-Neoproterozoic orogenic belts (Drysdall AR

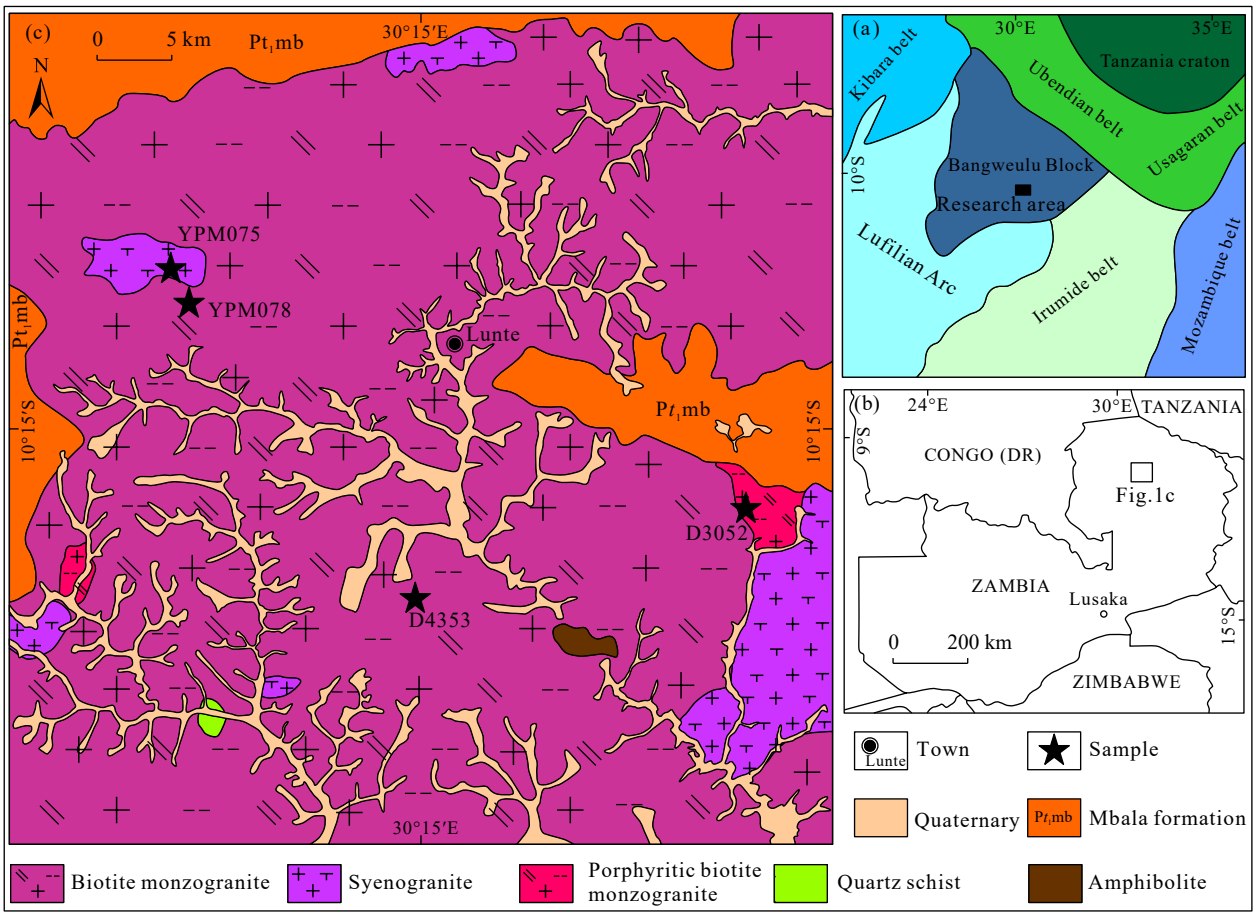

Fig. 1. Tectonic map (a, modified from De Waele B et al., 2008), location map (b) and regional geological map (c) of the Lunte area in northeastern Zambia.

et al., 1972; Andersen LS and Unrug R, 1984), including the Paleoproterozoic Ubendian-Usagaran Belt in the northeast, the Mesoproterozoic Kibara Belt, and the Neoproterozoic Lufilian Belt in the west (De Waele B et al., 2008), and the Mesoproterozoic Irumide Belt in the southeast (De Waele B et al., 2006b; Fig.1a).

The Bangweulu Block is mainly composed of the metamorphic crystalline basement and sedimentary cover. Generally, the crystalline basement includes granitic plutons, supracrustal sequences, and other intrusions (Andersen LS and Unrug R, 1984; Debruyne D et al., 2014). Among them, the granitoid is widely outcropped in the block as the most significant component of the basement, accounting for more than 50% of the entire block area (De Waele B et al., 2005, 2006a, 2006b; Ren JP et al., 2019a, 2019b; Zuo LB et al., 2020, 2021). The metamorphic supracrustal sequences mainly consist of schists and andesitic-rhyolitic metavolcanic. Banded schists are exposed in the eastern and northern parts of the Bangweulu Block, extending in a NW-SE or nearly EW direction (Saviaro K, 1979; Schandelmeier H, 1980). In terms of lithology, the schists mainly consist of micaceous or chloritic quartzo-feldapathic schists derived in part from acid volcanic or semipelitic - psammitic sediments (Andersen LS and Unrug R, 1984; Debruyne D et al., 2014). The metavolcanics are exposed along the present margins of the Mporokoso Basin, which is located centrally on the Bangweulu Block (Andersen LS and Unrug R, 1984). From bottom to top, the sedimentary units in the Bangweulu Block include the Paleoproterozoic Mporokoso Group, the Mesoproterozoic Kasama and Mansa River groups, the Neoproterozoic Katanga Supergroup, and the Cenozoic fluvial and lacustrine sediments. The Mporokoso Group unconformably overlies the basement and is the sedimentary cover that was deposited in the Bangweulu Block and the Irumide Belt after 2000 Ma (Daly M and Unrug R, 1982; Sun HW et al., 2019, 2021; Xing S et al., 2021).

3. Samples

In the study area, granite outcrops consist mainly of gray-white porphyritic biotite monzogranites, gray-white medium-fine-grained biotite monzogranites, gray medium-fine-grained biotite monzogranites, and gray-white fine-grained biotite syenogranites. This study conducted the whole-rock analysis and zircon U-Pb isotope dating of ubiquitous granitoid in the study area. The sampling locations are shown in Fig. 1c, and specific petrographic characteristics are described as follows.

Sample D3052 was collected from 30°26'31"E and 10°18'35"S, and it is a gray-white porphyritic biotite monzogranite with a porphyritic texture and a massive structure (Fig. 2a). The monzogranite mainly contains plagioclase, K-feldspar, quartz, and a small amount of biotite and garnets. The phenocrysts are 1 –6.5 mm in size, accounting for 58% of the entire sample. The matrix has a grain size of 0.3 –0.9 mm, accounting for 42% of the total composition. The composition of the matrix is essentially the same as that of the phenocrysts. The K-feldspar is mainly composed of microcline with well-developed crossed twinning, with a content of 36%. The plagioclase is semi-euhedral to anhedral and tabular in shape, with well-developed polysynthetic twinning and a content of 36%. The quartz is anhedral granular, colorless, and transparent, with well-developed intragranular cracks and a content of 22%. The biotite is semi-euhedral, flaky, and scaly, showing bright interference color and with a content of 5%. The garnets are anhedral granular, with well-developed intragranular cracks and a content of 1% (Fig. 2b).

Sample D4353 was collected from 30°14'55"E and 10°22'40"S, and it is a gray-white medium-fine-grained biotite monzogranite with a granular texture and a massive structure (Fig. 2c). The sample is mainly composed of K-feldspar, plagioclase, quartz, and a small amount of biotite and muscovite. The K-feldspar mainly includes perthite. It has a well-developed striped texture and is semi-euhedral to anhedral and platy in shape, with a particle size of 0.5 –4.8 mm and a content of 44%. The plagioclase is semi-euhedral to anhedral and platy in shape, with developed polysynthetic twinning. It has a particle size of 0.3–3.5 mm and a content of 28%. The quartz is anhedral granular, with developed intragranular cracks and showing parallel extinction in the whole rock. It has a particle size of 0.5–3.0 mm and a content of 21%. The biotite is light brown - dark brown semi-euhedral fine scales and shows strong pleochroism, with a content of 7% (Fig. 2d).

Sample YPM078 was collected from 30°7'27"E and 10°12'43"S, and it is a gray medium-fine-grained biotite monzogranite with a granular texture and a massive structure (Fig. 2e). The monzogranite mainly consists of K-feldspar, plagioclase, quartz, and a small amount of biotite, with silicification alteration being observed. The K-feldspar is dominated by semi-euhedral to anhedral and platy perthite with a well-developed striped texture. It has a particle size of 0.4 –5.2 mm and a content of 36%. The plagioclase is semi-euhedral and platy in shape and shows developed polysynthetic twinning. It has a particle size of 0.3 –4.5 mm and a content of 32%. The greasy quartz is distributed in anhedral granular aggregates, with a content of 24%. The light brown-dark brown biotite is semi-euhedral and fine-scale in shape. It shows strong polychromism, with a particle size of 0.25–0.98 mm and a content of 8% (Fig. 2f).

Sample YPM075 was collected from 30°6'44"E and 10°10'2"S, and it is a gray-white fine-grained syenogranite with a fine-grained texture and a massive structure (Fig. 2g). The syenogranite is mainly composed of K-feldspar, plagioclase, quartz, and a small amount of biotite. The K-feldspar is dominated by perthite and is semi-euhedral to anhedral and platy in shape, with a particle size of 1.02–2.85 mm. The K-feldspar is highly clayey overall, with a common striped texture and a content of 55%. The plagioclase is semi-euhedral and platy in shape and shows developed polysynthetic twinning, with a particle size of 1.00–1.78 mm and a content of 22%. The greasy quartz is distributed in anhedral granular aggregates. It shows parallel extinction, with a content of 20%. The biotite is semi-euhedral scaly and light brown-dark brown. It shows strong pleochroism, with a content of 3% (Fig. 2h).

Fig. 2. Hand specimen (a–D3052, c–D4353, e–YPM078, g–YPM075) and photomicrographs (b–D3052, d–D4353, f–YPM078, h–YPM075; crossed nicols) of granites from the Lunte area in northeastern Zambia. Q–quartz, Pl–plagioclase, Bt–biotite, Pth–perthite, Kfs–K-feldspar, Phl–phlogopite, Mc–microcline, Grt–garnet.

4. Analytical methods

Samples for Zircon U-Pb dating first underwent crushing, followed by panning and gravity, and magnetic sorting. Afterward, zircons were selected under a binocular microscope. These procedures were performed at the laboratory of Langfang Yuneng Rock Mineral Separation Technology Service Co. Ltd., Hebei Province, China. The target preparation and cathodoluminescence (CL) imaging and observation of zircons were performed at Beijing Gaonian Pilot Technology Co., Ltd. LA-ICP-MS Zircon U-Pb dating was performed at the laboratory of Tianjin Center, China Geological Survey. The instruments used include a 193 nm FXArF excimer laser ablation system from the New Wave Research and a Neptune multi-collector inductively-coupled plasma mass spectrometer (MC-ICP-MS) from Thermo Fisher Scientific. During the experiment, helium was used as the carrier gas for laser ablation, and the laser spot diameter was

set at approximately 35 μm. Specific operation conditions and detailed analysis process of relevant instruments were stated in Li HK et al. (2009). In the analysis process, isotope fractionation correction was conducted using Australian zircon standard GJ-1 as external reference standards. After the experiment, the ICPMSDataCal software was used to process data offline (Liu YS et al., 2010), and Ludwing KR (2003) was followed to plot U-Pb Concordia diagrams and calculate the weighted average U-Pb age.

The whole-rock analyses of major, trace, and rare earth elements were performed at the Element Analysis Laboratory of Tianjin Center, China Geological Survey. First, the sample powder was melted into a glass sheet, and then major elements were determined using an XRF 1500 X-ray fluorescence spectrometer. The analysis precision was better than 1%. FeO was dissolved in a mixed hydrofluoric and sulfuric acid dissolution and was determined using the potassium dichromate volumetric titration method, and the analysis accuracy was better than 2%. For the analysis of trace elements and rare earth elements (REEs), the sample solution was fully dissolved using high-purity HNO_3 and high-purity HF and then was diluted with 1% HNO_3. Finally, trace elements and REEs in the sample solution were determined using a double-focusing sector field inductively coupled plasma mass spectrometer (ICP-MS) from the Finnigan MAT company, and the analysis precision was better than 5%.

5. Results

5.1. Zircon U-Pb geochronology

In this study, zircon U-Pb dating was conducted on four granite samples from the Lunte area in northeastern Zambia. The CL images of some representative zircons are shown in Fig. 3, the zircon U-Pb concordia diagrams are illustrated in Fig. 4, and the analytical results are listed in Table 1.

In sample D3052, most zircons are columnar, with a particle size of 100 –150 μm and a length/width ratio of 3∶2 –3∶1. CL images show that most zircons have developed banded oscillatory zoning. The Th/U ratio of 30 analyzed spots varies from 0.14 to 1.19 and is high (> 0.4) mostly, indicating magmatic zircons (Belousova EA et al., 2002). The Th/U ratio of some zircons ranges from 0.1 to 0.4, which may reflect incomplete metamorphism and recrystallization (Wu YB and Zheng YF, 2004) or reformation induced by later geological events. Most of the analyzed spots deviate from the concordia curve and form inconsistent lines, and the upper intercept age is 2051±13 Ma.

In sample D4353, the zircon crystals are short columnar, with a particle size of approximately 60 –140 μm and a length/width ratio of approximately 2∶1 –3∶1. Zircon crystals exhibit banded oscillatory zoning and rarely exhibit core-rim textures. The Th/U ratio of 23 measuring spots is 0.01 –2.01 (> 0.4 mostly), which is consistent with typical magmatic zircons. The weighted average $^{207}Pb/^{206}Pb$ age is 2034±14 Ma (MSWD=0.05, n=8).

In sample YPM075, the zircon crystals are long columnar, with a particle size of 100 –210 μm and an aspect ratio of approximately 2∶1–4∶1. CL images show that most zircons have zoning textures and a few zircons have core-rim textures. The Th/U ratio of 20 zircon core measurement spots is 0.11 –2.16 and is high (> 0.4) mostly, reflecting the characteristics of magmatic zircons. The Th/U ratio of a small amount of zircon ranges from 0.1 to 0.4, which may reflect incomplete metamorphism and recrystallization (Wu YB and Zheng YF, 2004) or reformation induced by later geological events. Most of the analyzed spots deviate from the concordia curve to form inconsistent lines, and the upper intercept age is 2009±20 Ma.

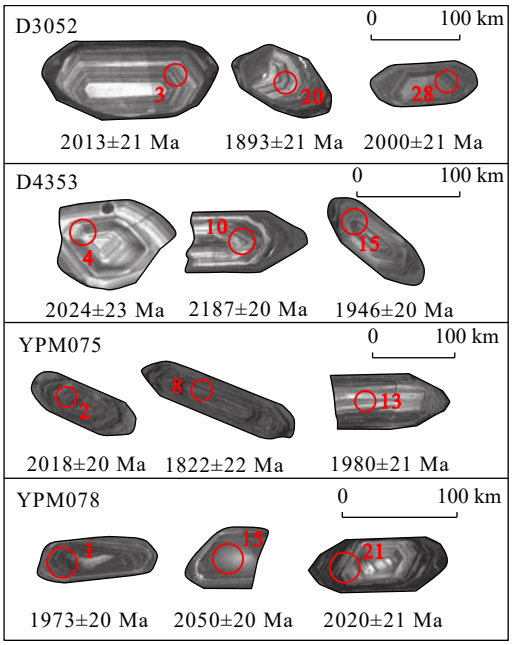

Fig. 3. Cathodoluminescence (CL) images and analytical spots of zircons from granites in the Lunte area in northeastern Zambia.

In sample YPM078, the zircon crystals are short columnar with core-rim textures. The grain size and length/width ratio of the zircons are 60–110 μm and approximately 1∶1–2∶1, respectively, and zoning textures can be observed. The Th/U ratio of 27 core measuring spots is 0.10 –2.71, which is consistent with that of typical magmatic zircons. Most of the analyzed spots deviate from the concordia curve to form inconsistent lines, and the upper intercept age is 2036±19 Ma.

5.2. Whole-rock geochemistry

The geochemical analysis results of granite samples from the Lunte area are given in Table 2. According to this table and the geochemical discrimination diagrams, granitoid do not show notable differences in geochemical characteristics, and different terranes show relatively consistent geochemical distribution characteristics. This indicates that they may have similar source areas and evolution mechanisms of magmas.

5.2.1. Major elements

The major element analysis results show that the SiO_2 content varies from 72.68% to 73.78% in different granitoid,

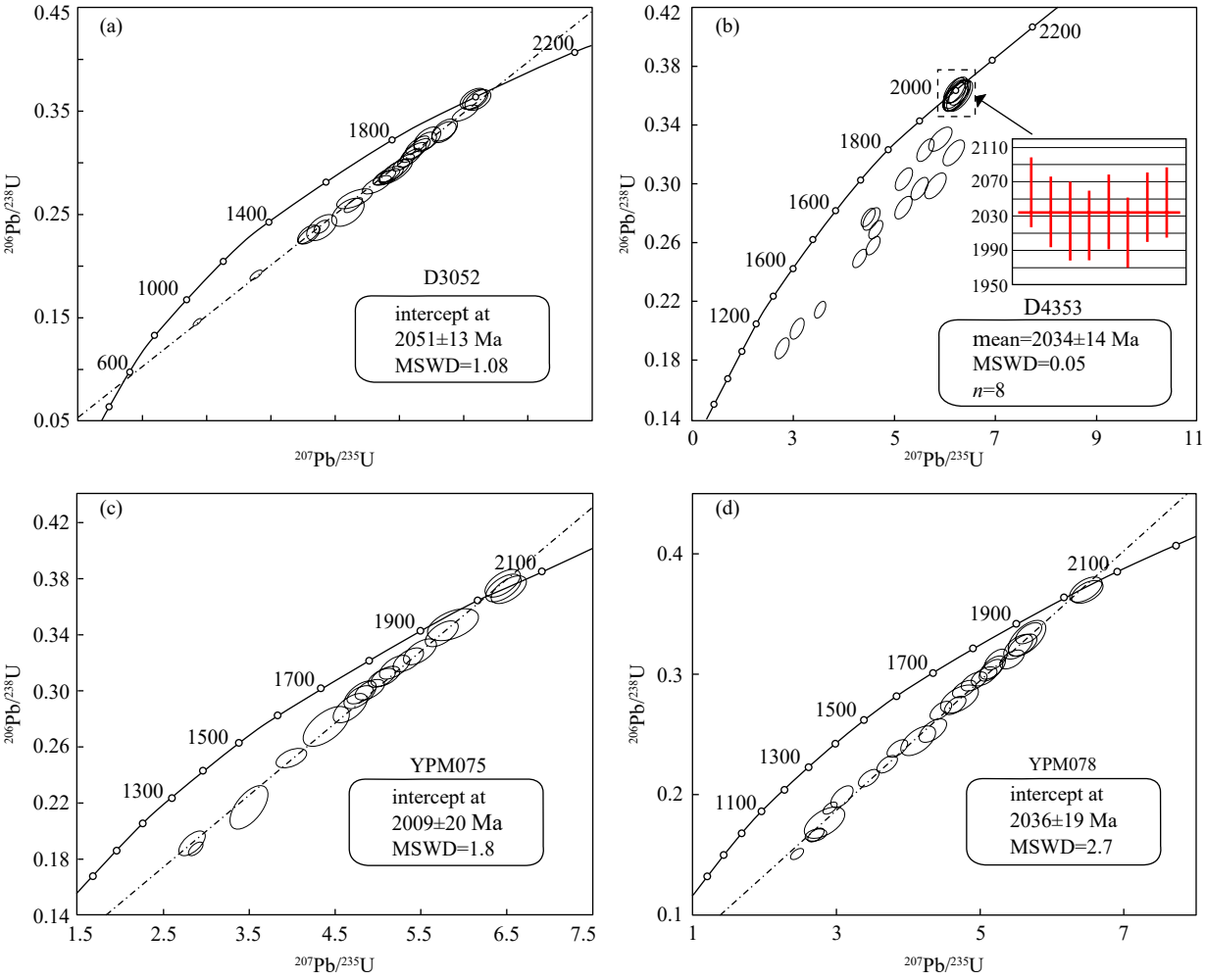

Fig. 4. Zircon LA-MC-ICP-MS U-Pb concordia diagrams for granites from the Lunte area in northeastern Zambia.

indicating the characteristics of typical acidic intrusive rocks. The samples from the Lunte area are relatively rich in potassium (K_2O = 5.14%–5.60%) and have high ALK [total alkali content (K_2O+Na_2O): 7.97% –8.27%], and their K_2O/Na_2O ratio is 1.82–2.29. In the TAS diagram of rock classification, all the sample spots fall into the granite zone (Fig. 5a). However, in the SiO_2-K_2O diagram, the sample spots fall into the high-K calc-alkaline to shoshonite zone, reflecting the high-K characteristics of rocks (Fig. 5b). The total iron content is 1.55%–2.50% in TFeO and 0.44%–0.66% in MgO. The Al_2O_3 content is 13.45% –14.76%, the Al saturation index A/CNK is 1.13–1.21, and the CIPW standard mineral calculation yielded 1.27% –1.95% of corundum molecules, exhibiting the characteristics of strongly peraluminous granites. In the A/NK-A/CNK diagram, all samples fall into the peraluminous zone representing S-type granites (Fig. 6). The results are slightly different from the samples (monzogranite and syenogranite) from the Kapatu area (Fig. 6).

5.2.2. Trace elements

The total REE content in all samples ranges from 212.05×10^{-6} to 611.23×10^{-6}. The fractionation of light and heavy REEs is obvious, showing a rightward inclination [Fig. 7a; (La/Yb) N = 5.95–33.57]. The samples are relatively rich in light rare earth elements (LREEs) and relatively depleted in heavy rare earth elements (HREEs). Meanwhile, they show noticeable negative Eu anomalies (Eu = 0.16 –0.40), suggesting that strong plagioclase segregation and crystallization may have occurred during diagenesis or that plagioclase existed in the residual phase of protolith melting. The primitive mantle-normalized trace element spidergram (Fig. 7b) shows that the samples are relatively enriched in large ion lithophilic elements (LILEs) such as Rb, Th, U, and K, and are relatively depleted in Ba, Sr, and high field strength elements (HFSE) such as Ta, Nb, and Ti.

Overall, different granite samples have the same distribution patterns of REEs and trace elements, indicating that they may have the same magma source areas. The comparison and analysis with the standard values of REEs and trace elements in the crust show that the granite samples are more similar to the upper crust, suggesting that its magma source areas may mainly include the upper crust.

6. Discussion

6.1. Emplacement age

To date, there are only a few geochronological data of the

Table 1. LA-MC-ICP-MS zircons U-Pb date of granites from the Lunte area in northeastern Zambia,

Samples and Anal. No.	$Th/10^{-6}$	$U/10^{-6}$	Th/U	$^{206}Pb/^{238}U$		$^{207}Pb/^{235}U$		$^{207}Pb/^{206}Pb$		$^{206}Pb/^{238}U$		$^{207}Pb/^{235}U$		$^{207}Pb/^{206}Pb$	
				Ratios	1σ	Ratios	1σ	Ratios	1σ	Age/Ma	1σ	Age/Ma	1σ	Age/Ma	1σ
YPM075															
1	19	31	0.61	0.3474	0.0047	5.8810	0.1295	0.1228	0.0033	1922	26	1958	43	1997	48
2	389	490	0.79	0.3767	0.0038	6.4532	0.0855	0.1243	0.0014	2061	21	2040	27	2018	20
3	477	687	0.69	0.2746	0.0059	4.3975	0.1137	0.1162	0.0014	1564	34	1712	44	1898	22
4	412	350	1.18	0.3726	0.0038	6.5127	0.0895	0.1268	0.0015	2042	21	2048	28	2054	21
5	860	867	0.99	0.2169	0.0062	3.4970	0.0920	0.1169	0.0017	1265	36	1527	40	1910	27
6	303	1384	0.22	0.1914	0.0034	2.8373	0.0623	0.1075	0.0013	1129	20	1365	30	1758	22
7	171	849	0.20	0.2520	0.0028	3.9903	0.0776	0.1148	0.0020	1449	16	1632	32	1877	31
8	593	1676	0.35	0.1873	0.0019	2.8759	0.0376	0.1114	0.0013	1107	11	1376	18	1822	22
9	66	145	0.46	0.2881	0.0042	4.6824	0.0833	0.1179	0.0016	1632	24	1764	31	1924	25
10	350	445	0.79	0.3221	0.0035	5.3539	0.0730	0.1205	0.0014	1800	19	1878	26	1964	20
11	2064	957	2.16	0.2992	0.0033	4.8194	0.0672	0.1168	0.0013	1688	18	1788	25	1908	21
12	292	411	0.71	0.3408	0.0035	5.7482	0.0789	0.1223	0.0014	1891	20	1939	27	1990	20
13	121	259	0.47	0.3273	0.0040	5.4899	0.0820	0.1216	0.0014	1825	22	1899	28	1980	21
14	128	730	0.17	0.3095	0.0032	5.0903	0.0682	0.1193	0.0014	1738	18	1834	25	1945	21
15	142	191	0.74	0.3738	0.0036	6.4625	0.0842	0.1254	0.0014	2047	20	2041	27	2034	20
16	432	657	0.66	0.3163	0.0037	5.1971	0.0767	0.1192	0.0014	1772	21	1852	27	1944	20
17	142	1335	0.11	0.2956	0.0034	4.7696	0.0702	0.1170	0.0013	1670	19	1780	26	1911	20
18	320	756	0.42	0.3092	0.0030	5.0453	0.0652	0.1183	0.0014	1737	17	1827	24	1931	20
19	110	163	0.67	0.3726	0.0037	6.4702	0.0851	0.1259	0.0014	2042	20	2042	27	2042	20
20	117	818	0.14	0.3008	0.0031	4.9048	0.0657	0.1183	0.0013	1695	17	1803	24	1930	20
YPM078															
1	253	607	0.42	0.3120	0.0035	5.2120	0.0738	0.1211	0.0014	1751	20	1855	26	1973	20
2	48	849	0.06	0.3055	0.0039	5.1755	0.0753	0.1229	0.0014	1718	22	1849	27	1999	21
3	94	716	0.13	0.1766	0.0056	2.8325	0.1144	0.1163	0.0016	1049	33	1364	55	1900	25
4	1459	2656	0.55	0.1507	0.0016	2.4490	0.0363	0.1179	0.0014	905	10	1257	19	1925	21
5	393	597	0.66	0.2942	0.0035	4.9121	0.0729	0.1211	0.0014	1662	20	1804	27	1973	20
6	500	1563	0.32	0.1983	0.0035	3.0752	0.0653	0.1125	0.0013	1166	21	1427	30	1840	21
7	385	992	0.39	0.2801	0.0046	4.7207	0.1116	0.1222	0.0016	1592	26	1771	42	1989	23
8	74	734	0.10	0.3121	0.0031	5.4423	0.0726	0.1265	0.0015	1751	17	1892	25	2049	20
9	68	247	0.27	0.3242	0.0038	5.5928	0.0822	0.1251	0.0014	1810	21	1915	28	2031	20
10	329	1254	0.26	0.3340	0.0035	5.6769	0.0803	0.1233	0.0014	1858	20	1928	27	2004	20
11	332	1390	0.24	0.1888	0.0019	2.9088	0.0387	0.1117	0.0013	1115	11	1384	18	1828	21
12	1194	2873	0.42	0.1668	0.0019	2.6972	0.0871	0.1173	0.0031	994	11	1328	43	1916	47
13	1158	427	2.71	0.3302	0.0060	5.6624	0.1037	0.1244	0.0015	1839	33	1926	35	2020	21
14	102	946	0.11	0.3228	0.0042	5.5305	0.0790	0.1243	0.0018	1804	23	1905	27	2018	25
15	445	389	1.15	0.3701	0.0044	6.4565	0.0955	0.1265	0.0014	2030	24	2040	30	2050	20
16	220	657	0.34	0.2981	0.0034	5.0555	0.0770	0.1230	0.0015	1682	19	1829	28	2000	22
17	37	1033	0.04	0.2698	0.0030	4.4527	0.0623	0.1197	0.0014	1540	17	1722	24	1952	20
18	46	137	0.34	0.2447	0.0050	4.1362	0.1075	0.1226	0.0015	1411	29	1661	43	1994	22
19	1023	913	1.12	0.2252	0.0028	3.7021	0.0556	0.1192	0.0014	1309	16	1572	24	1945	21
20	314	116	2.71	0.2873	0.0031	4.7804	0.0683	0.1207	0.0014	1628	18	1781	25	1966	21
21	747	606	1.23	0.2532	0.0040	4.3408	0.0794	0.1244	0.0014	1455	23	1701	31	2020	21
22	619	1883	0.33	0.1664	0.0024	2.7127	0.0466	0.1182	0.0014	992	14	1332	23	1930	21
23	313	660	0.47	0.2741	0.0029	4.6520	0.0636	0.1231	0.0014	1561	17	1759	24	2002	20
24	396	828	0.48	0.3030	0.0034	5.1345	0.0714	0.1229	0.0014	1706	19	1842	26	1999	21
25	571	430	1.33	0.2139	0.0028	3.4552	0.0597	0.1172	0.0014	1249	16	1517	26	1913	21
26	359	1418	0.25	0.2384	0.0026	3.8468	0.0556	0.1171	0.0014	1378	15	1603	23	1912	21
27	173	353	0.49	0.3683	0.0039	6.4835	0.0939	0.1277	0.0015	2022	21	2044	30	2066	21
D4353															
1	348	354	0.98	0.3600	0.0044	6.3062	0.0969	0.1271	0.0015	1982	24	2019	31	2058	20
2	55	219	0.25	0.3617	0.0036	6.2572	0.0829	0.1255	0.0014	1990	20	2012	27	2035	20
3	146	227	0.64	0.3210	0.0035	6.1724	0.0916	0.1394	0.0016	1795	20	2001	30	2220	20
4	68	86	0.79	0.3597	0.0036	6.1824	0.0875	0.1247	0.0016	1981	20	2002	28	2024	23
5	16	2630	0.01	0.2014	0.0032	3.0726	0.0586	0.1107	0.0013	1183	19	1426	27	1810	21

Table 1. (*Continued*)

Samples and Anal. No.	Th/10^{-6}	U/10^{-6}	Th/U	$^{206}Pb/^{238}U$		$^{207}Pb/^{235}U$		$^{207}Pb/^{206}Pb$		$^{206}Pb/^{238}U$		$^{207}Pb/^{235}U$		$^{207}Pb/^{206}Pb$	
				Ratios	1σ	Ratios	1σ	Ratios	1σ	Age/Ma	1σ	Age/Ma	1σ	Age/Ma	1σ
6	32	201	0.16	0.3620	0.0043	6.2043	0.0913	0.1243	0.0014	1992	24	2005	30	2019	20
7	218	275	0.79	0.2579	0.0026	4.5761	0.0618	0.1287	0.0015	1479	15	1745	24	2080	21
8	191	232	0.82	0.3600	0.0036	6.2262	0.0857	0.1254	0.0016	1982	20	2008	28	2035	22
9	178	402	0.44	0.2687	0.0027	4.6297	0.0620	0.1250	0.0015	1534	15	1755	23	2028	21
10	158	411	0.39	0.2965	0.0037	5.5944	0.0828	0.1368	0.0016	1674	21	1915	28	2187	20
11	212	541	0.39	0.3303	0.0033	5.9089	0.0920	0.1297	0.0017	1840	18	1963	31	2094	23
12	108	680	0.16	0.2143	0.0022	3.5257	0.0472	0.1193	0.0014	1251	13	1533	21	1946	20
13	225	1427	0.16	0.2771	0.0027	4.4775	0.0584	0.1172	0.0013	1577	16	1727	23	1914	20
14	57	306	0.19	0.3228	0.0032	5.6122	0.0741	0.1261	0.0014	1804	18	1918	25	2044	20
15	105	967	0.11	0.2760	0.0031	4.5418	0.0692	0.1193	0.0014	1571	18	1739	26	1946	21
16	222	2508	0.09	0.1952	0.0021	3.5740	0.0516	0.1328	0.0016	1150	12	1544	22	2135	21
17	258	233	1.10	0.3068	0.0034	5.1224	0.0700	0.1211	0.0014	1725	19	1840	25	1973	21
18	2556	3401	0.75	0.1880	0.0028	2.7747	0.0524	0.1071	0.0013	1110	17	1349	25	1750	22
19	432	488	0.89	0.2837	0.0033	5.1767	0.0754	0.1323	0.0015	1610	19	1849	27	2129	20
20	468	443	1.06	0.2492	0.0027	4.3121	0.0587	0.1255	0.0014	1434	15	1696	23	2036	20
21	696	347	2.01	0.3623	0.0040	6.1806	0.0862	0.1237	0.0014	1993	22	2002	28	2011	20
22	49	171	0.29	0.3593	0.0040	6.2316	0.0890	0.1258	0.0014	1979	22	2009	29	2040	20
23	109	189	0.57	0.3613	0.0039	6.2879	0.0875	0.1262	0.0015	1988	22	2017	28	2046	20
D3052															
1	255	336	0.76	0.3624	0.0038	6.1519	0.0847	0.1231	0.0014	1994	21	1998	28	2002	20
2	185	404	0.46	0.3170	0.0034	5.2804	0.0723	0.1208	0.0014	1775	19	1866	26	1968	20
3	158	185	0.85	0.3623	0.0036	6.1891	0.0838	0.1239	0.0015	1993	20	2003	27	2013	21
4	159	593	0.27	0.2306	0.0038	3.5886	0.0730	0.1128	0.0013	1338	22	1547	31	1846	21
5	69	309	0.22	0.3297	0.0039	5.6931	0.0845	0.1252	0.0014	1837	22	1930	29	2032	20
6	218	1408	0.15	0.1456	0.0015	1.8562	0.0252	0.0925	0.0011	876	9	1066	14	1477	22
7	72	225	0.32	0.2788	0.0037	4.6464	0.0903	0.1209	0.0016	1586	21	1758	34	1969	23
8	54	330	0.16	0.3113	0.0032	5.2439	0.0717	0.1222	0.0014	1747	18	1860	25	1988	21
9	193	809	0.24	0.2585	0.0028	4.2767	0.0582	0.1200	0.0014	1482	16	1689	23	1956	21
10	414	467	0.88	0.3601	0.0036	6.2003	0.0824	0.1249	0.0014	1983	20	2004	27	2027	20
11	434	1188	0.37	0.1915	0.0020	2.7685	0.0376	0.1049	0.0012	1130	12	1347	18	1712	21
12	80	296	0.27	0.3226	0.0047	5.4283	0.0842	0.1220	0.0015	1802	26	1889	29	1986	21
13	187	686	0.27	0.3004	0.0031	5.0611	0.0681	0.1222	0.0014	1693	18	1830	25	1988	21
14	192	341	0.56	0.2880	0.0037	4.8794	0.0768	0.1229	0.0015	1631	21	1799	28	1999	21
15	331	324	1.02	0.2854	0.0030	4.7674	0.0646	0.1211	0.0014	1619	17	1779	24	1973	20
16	112	574	0.19	0.2651	0.0042	4.3021	0.1167	0.1177	0.0019	1516	24	1694	46	1921	29
17	109	265	0.41	0.3325	0.0039	5.6991	0.0785	0.1243	0.0018	1851	22	1931	27	2019	26
18	229	776	0.29	0.2878	0.0030	4.8454	0.0681	0.1221	0.0014	1631	17	1793	25	1987	21
19	378	1104	0.34	0.2306	0.0029	3.5773	0.0648	0.1125	0.0014	1338	17	1545	28	1840	22
20	173	1273	0.14	0.2374	0.0050	3.7916	0.0919	0.1159	0.0013	1373	29	1591	39	1893	21
21	229	438	0.52	0.3051	0.0034	5.1632	0.0718	0.1227	0.0014	1716	19	1847	26	1996	21
22	147	225	0.65	0.3195	0.0041	5.3709	0.0853	0.1219	0.0014	1787	23	1880	30	1985	20
23	53	240	0.22	0.3618	0.0036	6.1734	0.0824	0.1238	0.0015	1991	20	2001	27	2011	21
24	236	350	0.67	0.2382	0.0024	3.7791	0.0503	0.1150	0.0013	1378	14	1588	21	1881	21
25	197	269	0.73	0.3147	0.0035	5.2875	0.0734	0.1219	0.0014	1764	20	1867	26	1984	20
26	276	266	1.04	0.3611	0.0039	6.2079	0.0840	0.1247	0.0014	1987	22	2006	27	2024	20
27	69	113	0.61	0.2947	0.0034	4.9795	0.0752	0.1225	0.0015	1665	19	1816	27	1994	21
28	228	191	1.19	0.2933	0.0044	4.9720	0.0851	0.1230	0.0014	1658	25	1815	31	2000	21
29	70	137	0.51	0.3482	0.0035	6.0217	0.0820	0.1254	0.0015	1926	20	1979	27	2035	21
30	163	356	0.46	0.2521	0.0052	4.1977	0.1065	0.1207	0.0015	1449	30	1674	42	1967	22

Bangweulu Block, and those early age data suffered low accuracy. The earliest age results obtained are the whole rock Rb-Sr isochron ages of granites and volcanic rocks in the Mansa area in the western part of the Bangweulu Block, which is 1833±18 Ma and 1812±22 Ma, respectively (Brewer MS et al., 1979). Subsequently, the whole rock Rb-Sr isochron age of Kate granite (1839±80 Ma; Schandelmeier H, 1980) was reported from the northern part of the Bangweulu Block. In recent years, Ren JP et al. (2019a, b) and Zuo LB et al. (2020) have reported new ages of the western Kasama

Table 2. Major elements (%) and trace elements (10^{-6}) compositions of granites from the Lunte area in northeastern Zambia.

Sample No.	YPM075	YPM078	D3052	D4353	Sample No.	YPM075	YPM078	D3052	D4353
SiO_2	73.26	72.68	73.78	72.72	Be	3.79	1.36	2.26	4.12
Al_2O_3	14.26	13.66	13.45	14.76	Sc	4.28	7.44	9.73	4.1
TiO_2	0.22	0.45	0.29	0.25	V	11.8	20.3	10.9	11.3
Fe_2O_3	0.32	0.84	0.6	0.58	Cr	8.68	6.31	6.98	10.8
FeO	1.34	1.74	1.32	1.03	Co	2.7	3.96	2.68	2.62
CaO	0.9	0.64	0.9	1.08	Ni	4.32	3.56	2.87	4.76
MgO	0.44	0.66	0.45	0.47	Ga	16.8	17.6	14.6	16.2
K_2O	5.35	5.6	5.35	5.14	Rb	290	324	348	328
Na_2O	2.92	2.45	2.7	2.83	Sr	105	112	68.2	118
MnO	0.04	0.04	0.07	0.04	Zr	113	239	155	125
P_2O_5	0.11	0.11	0.12	0.12	Nb	10.8	22	18.8	12.2
LOI	0.69	0.96	0.83	0.87	Mo	1.39	0.84	0.58	0.52
Total	99.85	99.83	99.86	99.89	Y	16.7	40.2	50.6	24.5
Mg#	32.73	32.25	30.34	35.28	La	47.1	119	49.6	43.8
Na_2O+K_2O	8.27	8.05	8.05	7.97	Pr	11.6	35	13	10.9
K_2O/Na_2O	1.83	2.29	1.98	1.82	Nd	41.7	132	47.9	39.6
A/NK	1.34	1.35	1.31	1.44	Sm	8.24	25.7	10.7	7.98
A/CNK	1.16	1.21	1.13	1.21	Eu	0.74	1.23	0.75	0.97
T(FeO)	1.63	2.5	1.86	1.55	Gd	6.28	18.8	9.41	6.42
$T(Fe_2O_3)$	1.81	2.77	2.07	1.72	Tb	0.85	2.48	1.55	0.96
Cs	3.7	4.04	2.23	4.86	Ce	98.5	258	109	90.5
Ba	342	474	377	428	Dy	3.76	10.5	9.33	4.95
Hf	3.9	7.68	5.46	4.43	Ho	0.63	1.64	1.86	0.92
Ta	0.92	0.9	0.96	1.29	Er	1.52	3.73	5.3	2.42
W	0.59	0.37	0.36	0.46	Tm	0.2	0.42	0.83	0.33
Pb	39	51.1	43	43.1	Yb	1.14	2.39	5.62	2.01
Th	35	140	38.5	28.9	Lu	0.17	0.34	0.84	0.29
U	5.1	4.55	6.05	3.74	∑LREE	207.88	570.93	230.95	193.75
Sn	2.01	1.76	1.38	2.9	∑HREE	14.55	40.3	34.74	18.3
Li	17.9	17.8	29.1	28.7	δEu	0.3	0.16	0.22	0.4

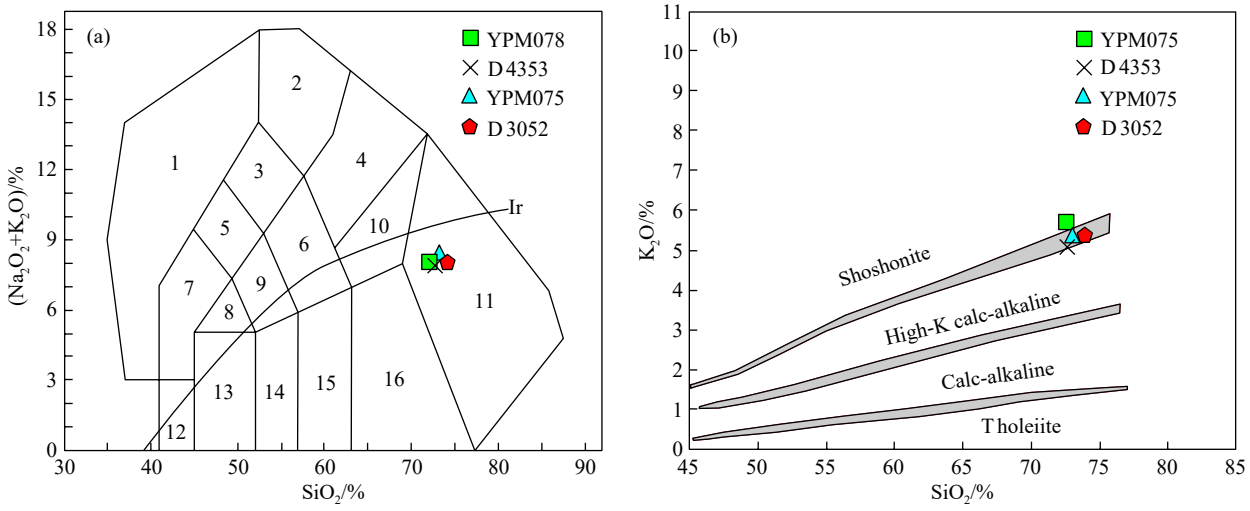

Fig. 5. TAS diagram (a, after Irvine TH and Baragar WR, 1971) and K_2O-SiO_2 diagram (b, after Rollinson HR, 1993) of granites from the Lunte area in northeastern Zambia. 1–foidolite, 2–foid syenite, 3–foid monzosyenite, 4–syenite, 5–foid monzodiorite, 6–monzonite, 7–foid gabbro, 8–monzogabbro, 9–monzodiorite, 10–quartz monzonite, 11–granite, 12–peridotgabbro, 13–gabbro, 14–gabbroic diorite, 15–diorite, 16–granodiorite.

granitoid (1964±8 Ma–2011±20 Ma) obtained using the LA-MC-ICP-MS zircon U-Pb dating method, and they are similar to the formation age of the granites in the Kapatu area (2012±11 Ma –1970±20 Ma; Gu AL et al., 2021). However, there is nearly no geochronological data of basement granitoid in the Lunte area. The geochronological data from this study show that the emplacement age of the granitoid in the Lunte area varies between 2009±20 Ma and 2051±13 Ma, which is

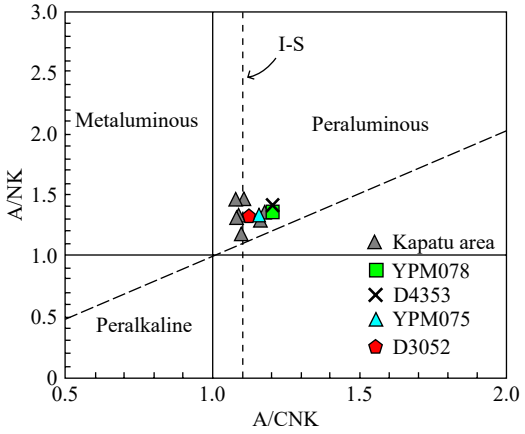

Fig. 6. A/NK *vs*. A/CNK diagram of granites from the Lunte area in northeastern Zambia (after Maniar PD and Piccoli PM, 1989; data of the Kapatu area from Gu AL et al., 2021).

also consistent with the basement formation age obtained by previous studies and belongs to the Early Paleoproterozoic.

Based on the regional tectonic evolution, De Waele B et al. (2006a) divided the magmatic-tectonic events in the Bangweulu Block into six stages, namely the Pre-Usagaran period (> 2100 Ma), Usagaran period (2050 –1950 Ma), Ubendian period (1950 –1880 Ma), Post-Ubendian period (1880 –1650 Ma), Lukamfwa period (1650 –1550 Ma), and Irumide period (1080 –850 Ma). The zircon ages of four samples range from 2051±13 Ma to 2009±20 Ma, belonging to the Usagaran period. Therefore, the authors believe that the most robust magmatism in the Lunte area occurred during the Usagaran period, which is consistent with the previous conclusion drawn from the statistical data on the distribution patterns of the detrital zircon U-Pb ages of the sedimentary cover (the Mporokso Group; De Waele B et al., 2006a, 2006b; Sun HW et al., 2019, 2021). In addition, the presence of some zircon ages of the Usagaran period implies that the crustal growth of the Bangweulu Block must have occurred before ca. 2000 Ma since it was followed by the deposition of the sedimentary sequences —the Mporokoso Group (2000 Ma). This is consistent with the conclusion of this study that the crystalline basement age is older than 2000 Ma.

6.2. Petrogenesis

Granites can be divided into types I, S, A, and M according to their genetic types (Chappell BW and White AJR, 1974). The granitoid in the Lunte area are characterized by high silicon (SiO_2 = 72.68% –73.78%), high aluminum (Al_2O_3 = 13.45%–14.76%), rich potassium (K_2O/Na_2O = 1.82–2.29), low phosphorus (P_2O_5 = 0.11%–0.12%), and depleted magnesium (MgO=0.44% –0.66%), with an aluminum saturation index (A/CNK) of 1.13 –1.21 and a CIPW corundum standard molecular index of greater than 1% (1.27%–1.95%). The trace element analysis shows that there are relatively low contents of Cr (6.31×10^{-6}–10.8×10^{-6}), Ni (2.87×10^{-6}–4.76×10^{-6}), and Co (2.62×10^{-6}–3.96×10^{-6}), exhibiting the geochemical characteristics of crustal sources.

Generally, A-type granites have a higher 10000×Ga/Al ratio and Nb content than I- and S-type granites (Whalen JB et al., 1987). Granites from the Lunte area have a low 10000*Ga/Al ratio and Nb content. In the A-type granite discriminant diagram, all the samples fall into the zone representing I+S-type granites (consistent with the samples from the Kapatu area) and are notably different from the A-type granites (Fig. 8a). In addition, some studies showed that Th and Y contents, as well as their correlation with Rb, are important reference indices for distinguishing S-type granites from I-type granites (Chappell BW, 1999). In the genetic-type diagram of granites, all samples from the Lunte area fall into the zone representing S-type granites (Fig. 8b). Typically, Th, Y, and Rb of S-type granites are negatively correlated, while Th, Y, and Rb of I-type granites are positively correlated. The Th, Y, and Rb of granites in the Lunte area are notably negatively correlated, suggesting the affinity with S-type granites (Figs. 8c, d). According to mineralogical studies,

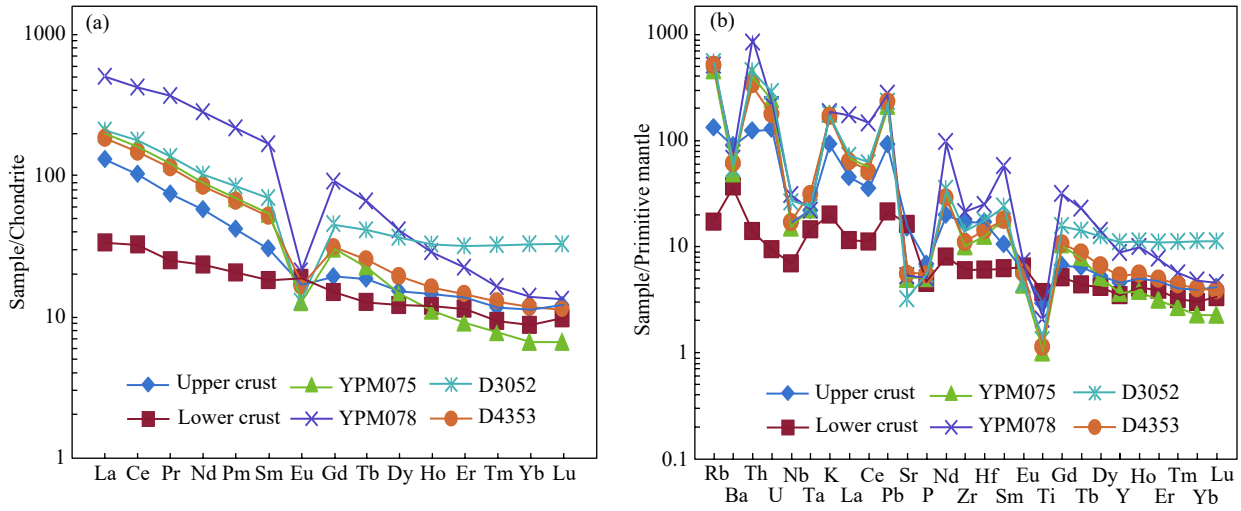

Fig. 7. Chondrite-normalized REE element patterns (a) and primitive mantle-normalized trace element spidergram (b) of granites from the Lunte area in northeastern Zambia (chondrite and primitive mantle normalizing values from Sun SS and McDonough WF, 1989, crust contents after Taylor SR and McLennan SM, 1985).

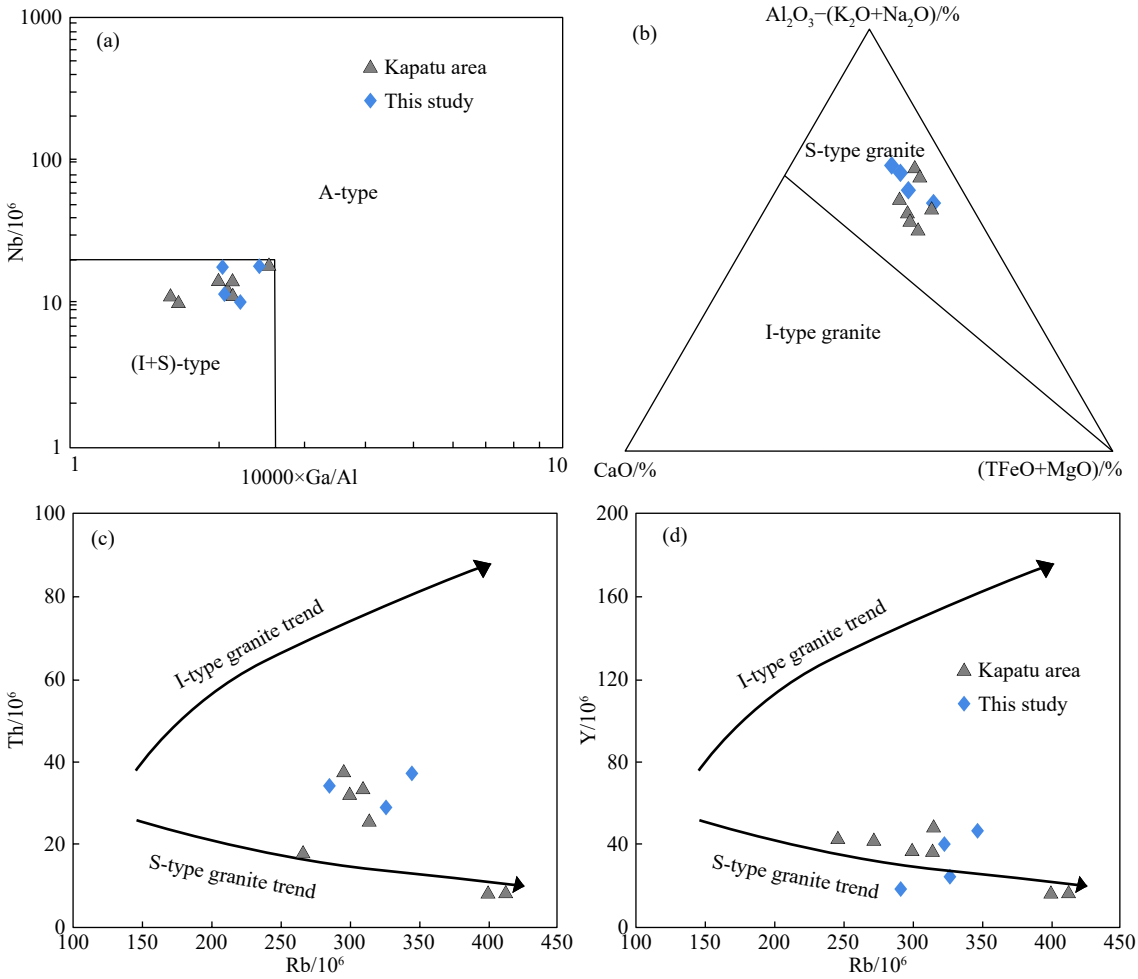

Fig. 8. 10000×Ga/Al *vs.* Nb (a, modified from Whalen JB et al., 1987), Al_2O_3-(K_2O+Na_2O) *vs.* CaO–TFeO+MgO (b, modified from White AKR and Chappell BW, 1977), Rb *vs.* Th (c) and Rb–Y (d; c and d after Chappell BW and White AJR, 1999) diagrams of granites from the Lunte area in northeastern Zambia (data of the Kapatu from Gu AL et al., 2021).

garnets, muscovite, and other aluminum-rich minerals are common in granitoid in the Lunte area, which is consistent with the characteristics of S-type granites. Based on the above analysis, similar to the granites from the Kapatu area, the Paleoproterozoic granites that are widely developed in the Lunte area most likely belong to peraluminous S-type granites.

6.3. Magma source

S-type granites are commonly interpreted as magmas derived from the partial melting of metasedimentary crust (Sylvester PJ, 1998). Experimental petrological studies show that the CaO/Na_2O ratio of S-type granites formed from the partial melting of different source areas notably differs (Sylvester PJ, 1998). It is relatively low (< 0.3) for S-type granites formed from the remelting of argillaceous rocks but is relatively high (> 0.3) for S-type granites formed from the remelting of sandy rocks. The CaO/Na_2O ratio of granite samples in the study area is 0.26–0.38, with an average of 0.32, from which no obvious indication of source areas can be deduced. However, as shown in the discrimination diagram of granite source areas (Fig. 9a), most of the granite samples fall into the partially melting zone of metamorphic argillaceous rocks. In the mixed simulation results of argillaceous rock and basalt melting, the samples fall into the zone close to argillaceous rock melting, and all samples show the characteristics of the clay-rich source zone (Fig. 9b). In addition, the characteristics of REEs and trace elements are very similar to those of the upper crust. Therefore, comprehensive analysis shows that the source areas of granite magmas in the Lunte area are mainly formed by the partial melting of crustal argillaceous rocks. However, some samples in the Kapatu area fell into the melting zone of metamorphic gray sandstones, indicating that the Bangweulu Block has diverse granite source areas.

6.4. Tectonic setting

The collision between the Bangweulu Block and the Tanzania Craton during the Paleoproterozoic led to the formation of the Usagaran-Ubendian orogenic Belt, but the regional tectonic evolution is still controversial. Brewer MS et al. (1979) claimed that the high-K calc-alkaline felsic igneous rocks developing at 1850 Ma in the Bangweulu Block represent an active continental margin arc environment related

to the Ubendian orogenic belt. Andersen LS and Unrug R (1984) believed that the metamorphic volcanic rocks related to the high-K calc-alkaline series in the northwestern Bangweulu Block were formed in a subduction system. De Waele B et al. (2006) and Sun HW et al. (2019) argued that the northeastern Bangweulu Block was in a passive continental margin environment during the Proterozoic. Kazimoto EO et al. (2015) suggested that many collisions occurred between the Bangweulu Block and the Tanzania Craton during the Paleoproterozoic and that the entire area was in a continent-continent collision environment. Ren JP et al. (2019a) suggested that the Bangweulu Block might have been formed in an Andean-type active continental margin environment.

The Lunte area is located in the central part of the Bangweulu Block. The granitic intrusions widely exposed in the area are the major components of the basement complex in the Bangweulu Block. This study shows that the granites in the study area likely formed between 2051±13 Ma and 2009±20 Ma during the Paleoproterozoic and constitute a peraluminous S-type granite as a whole. Generally, the formation of S-type granites is usually related to collisional orogeny and they may be formed in syn-collision and post-collision environments (Sylvester PJ, 1998; Barbarin B, 1999). According to the source analysis, the granites in the Lunte area resulted from the partial melting of crustal argillaceous rocks, while the melting of crust-derived metamorphic clastic rocks is one of the main processes for the generation of granitoid during the collisional orogeny (Zhou TF et al., 2010). As shown in the R1 vs. R2 tectonic environment diagram, all the samples fall into the zone of syn-collisional granites derived from crust melting (Fig. 10a). Meanwhile, in the (Y+Nb) *vs.* Rb diagram, all the samples fall in the syn-collisional or post-collisional granite zone (Fig. 10b), and data from the Kapatu area show similar characteristics (Gu AL et al., 2021). From a regional perspective, Lenoir JL et al. (1994) believed that the collision between the Tanzania Craton and the Bangweulu Block at

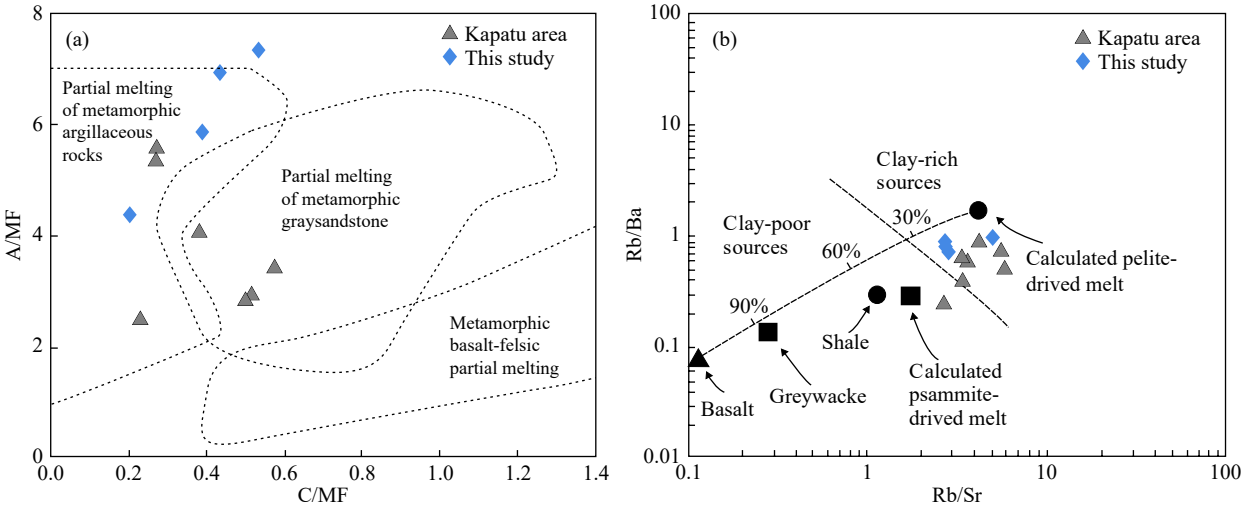

Fig. 9. A/MF *vs.* C/MF diagram (a) and Rb/Ba *vs.* Rb/Sr diagram (b) of granites from the Lunte area in northeastern Zambia (a, after Altherr R et al., 2000; b, after Sylvester PJ, 1998; data of the Kapatu area are quoted from Gu AL et al., 2021).

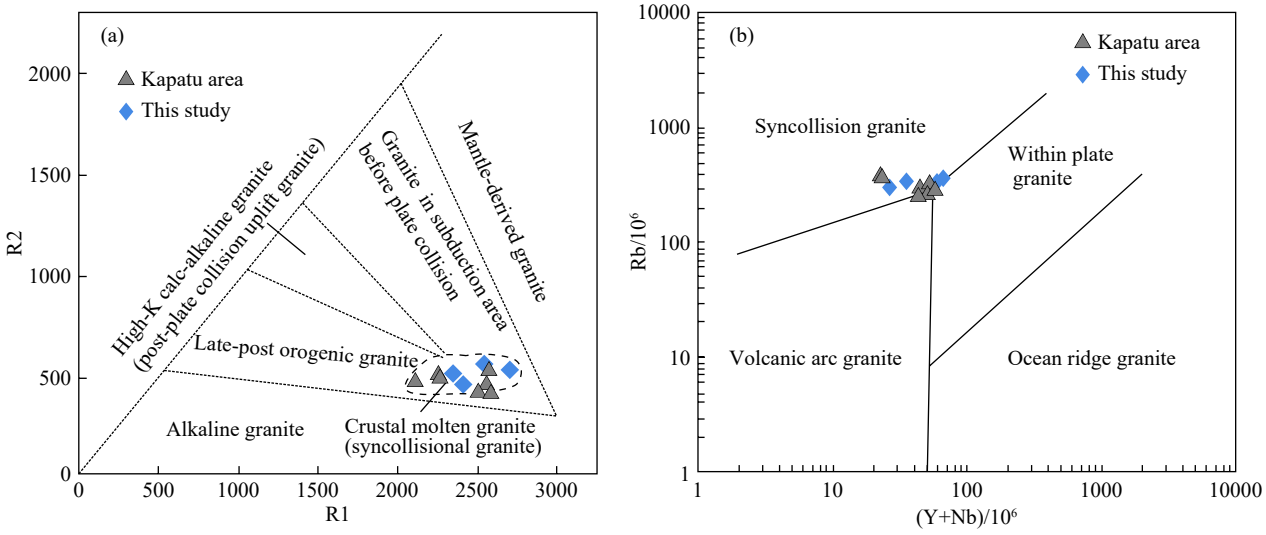

Fig. 10. R1 *vs.* R2 diagram (a) and Rb *vs.* (Y+Nb) diagram (b) of granites from the Lunte area in northeastern Zambia (a, after Batchelor RA and Bowden P, 1985; b, after Pearce JA et al., 1984; data of the Kapatu area from Gu AL et al., 2021).

2100–2025 Ma corresponds to the early collisional orogenic event in the Ubendian Belt. Meanwhile, the formation age of eclogites in the Paleoproterozoic Usagaran Belt in Tanzania is 2010–1996 Ma, which also reflects the collisional orogeny of about 2.0 Ga (Möller A et al., 1995). Boniface N and Schenk V (2012) suggested that the Usagaran Belt was in a continental collision stage during 2.05–1.93 Ga.

The comprehensive study indicates that the granites in the Lunte area were likely formed in the collision environment between the Bangweulu Block and Tanzania Craton. Combining this with the emplacement age of granites in the area, the authors suggest that the granites in the Lunte area are mainly the product of the Usagaran orogeny, which is also the main formation period of the Bangweulu Block.

During the Paleoproterozoic-Mesoproterozoic Columbia supercontinent cycle, many large-scale collisional orogenic events occurred in the world, including the Eburnean orogeny (2.10–2.00 Ga), the Limpopo orogeny (2.00–1.90 Ga), the Capricorn orogeny (2.00–1.85 Ga), and the intracontinental collisional orogeny of the North China Craton (1.85 Ga; Cooper MR, 1990; Zhao GC et al., 2002; Rogers JJW and Santosh M, 2002; Zhai MG, 2010; Smit CA et al., 2014; Sun K et al., 2018). This study shows that the extensively developing granites in the Lunte area, northeastern Zambia were formed during 2.00 –2.05 Ga under a tectonic environment of syn-collision or post-collision.

Therefore, the authors infer that the Paleoproterozoic magmatic event in the Bangweulu Block may be the response of the block to the Columbia supercontinent convergence. Further research on the convergence mechanisms is required.

7. Conclusions

(i) The granitoid in the Lunte area, northeastern Zambia were formed during the Paleoproterozoic, with an emplacement age of 2051±13 –2009±20 Ma, which is consistent with the Usagaran tectonic event.

(ii) The whole-rock geochemical characteristics show that the granitoid in the Lunte area, northeastern Zambia belongs to strongly peraluminous S-type granites, and the distribution characteristics of trace elements and REEs are similar to those of the upper crust. It is suggested that the source rocks of the granites originated from the partial melting of crustal argillaceous rocks.

(iii) The granitoid in the study area is the product of the collisional environment between the Bangweulu Block and the Tanzania Craton. Based on the history of global tectonic evolution, the authors conclude that the Bangweulu Block may be a part of the Columbia supercontinent, and the magmatism in the study area might belong to the geological response of the Bangweulu Block to the collision orogeny of the Columbia supercontinent.

CRediT authorship contribution statement

Hong-wei Sun conceived of the presented idea. Hong-wei Sun wrote the manuscript with support from Jun-ping Ren. Jun-ping Ren improved the theory. All authors discussed the results and contributed to the final manuscript.

Declaration of competing interest

The authors declare no conflicts of interest.

Acknowledgment

This study was jointly funded by projects of the Ministry of Commerce ([2015] 352 and [2012]558) and the projects of the China Geological Survey (DD20201150 and 1212011220910). Thoughtful comments by three anonymous reviewers and editors have considerably improved the manuscript.

References

Altherr R, Holl A, Hegner E, Langer C, Kreuzer H. 2000. High-potassium, calc-alkaline I-type plutonism in the European Variscides: Northern Vosges and northern Schwarzwald. Lithos, 50(1/3), 51–73. doi: 10.1016/S0024-4937(99)00052-3.

Armstrong RA, Master S, Robb LJ. 2005. Geochronology of the Nchanga granite, and constraints on the maximum age of the Katanga Supergroup, Zambian Copperbelt. Journal of African Earth Sciences, 42(1/5), 32–40. doi: 10.1016/j.jafrearsci.2005.08.012.

Andersen LS, Unrug R. 1984. Geodynamic evolution of the Bangweulu Block, northern Zambia. Precambrian Research, 25(1/3), 187–212.

Belousova EA, Griffin WL, Reilly SY, Fisher N. 2002. Igneous zircon: Trace element composition as an indicator of source rock type. Contributions to Mineralogy and Petrology, 143, 602–622. doi: 10.1007/s00410-002-0346-7.

Brewer MS, Haslam HW, Darbyshire DPF, Davis AE. 1979. Rb-Sr age determination in the Bangweulu Block, Luapula Province, Zambia. Institute of Geological Science, 79(5), 11.

Barbarin B. 1999. A review of the relationships between granitoid types, their origins and their geodynamic environments. Lithos, 46(3), 605–626. doi: 10.1016/S0024-4937(98)00085-1.

Batchelor RA, Bowden P. 1985. Petrogenetic interpretation of granitoid rock seires using multicationic parameters. Chemical Geology, 48, 43–55. doi: 10.1016/0009-2541(85)90034-8.

Boniface N, Schenk V. 2012. Neoproterozoic eclogites in the Paleoproterozoic Ubendian Belt of Tanzania: Evidence for a Pan-African suture between the Bang-Weulu Block and the Tanzania Craton. Precambrian Research, 208/211, 72–89. doi: 10.1016/j.precamres.2012.03.014.

Chappell BW, White AJR. 1974. Two contrasting granite types. Pacific Geology, 8, 173–174.

Chappell BW. 1999. Aluminium saturation in I- and -S type granites and the characterization of fractionated haplogranites. Lithos, 46(3), 535–551. doi: 10.1016/S0024-4937(98)00086-3.

Cooper MR. 1990. Tectonic cycles in southern Africa. Earth Science Reviews, 28(4), 321–364. doi: 10.1016/0012-8252(90)90053-X.

De Waele B, Johnson SP, Nkemba S, Tembo F. 2005. High-temperature, low-pressure tectono-thermal evolution of the Irumide belt, central, Southern Africa: Lithosphere delamination during arc-accretion. Frontier Research on Earth Evolution Report, 2004(2), 1–9.

De Waele B, Liégeois JP, Nemchin AA, Tembo F. 2006a. Isotopic and geochemical evidence of Proterozoic episodic crustal reworking within the Irumide Belt of south-central Africa, the southern metacratonic boundary of an Archaean Bangweulu Craton. Precambrian Research, 148(3), 225–256. doi: 10.1016/j.precamres.

2006.05.006.

De Waele B, Kampunzu AB, Mapani BSE, Tembo F. 2006b. The Mesoproterozoic Irumide belt of Zambia. Journal of African Earth Sciences, 46(1), 36–70.

De Waele B, Johnson SP, Pisarevsky SA. 2008. Palaeoproterozoic to Neoproterozoic growth and evolution of the eastern Congo Craton: Its role in the Rodinia puzzle. Precambrian Research, 160(1), 127–141.

Debruyne D, Van Wilderode J, Balcaen L, Vanhaecke F, Muchez P. 2014. Geochemistry and isotopic evolution of the central African Domes, Bangweulu and Irumide regions: Evidence for cryptic Archean sources and a Paleoproterozoic continental arc. Journal of African Earth Sciences, 100, 145–163. doi: 10.1016/j.jafrearsci.2014.06.013.

Daly M, Unrug R. 1982. The Muva Supergroup of northern Zambia: A craton to orogenic belt sedimentary sequence. Geological Society of South Africa, 85(3), 155–165.

Drysdall AR, Johnson RL, Moore TA, Thieme JG. 1972. Outline of the geology of Zambia. Geology Mijnbouw, 51, 265–276.

Irvine TH, Baragar WR. 1971. A guide to the chemical classification of the common volcanic rocks. Canadian Journal of Earth Sciences, 8, 523–548. doi: 10.1139/e71-055.

Gu AL, Wang J, Ren JP, Zuo LB, Sun HW, Xing S, Liu ZJ, Chikambwe EM. 2020. Geological characteristics and mineralization potential analysis for the Pan-African Hook Batholith in Central Zambia. Geological Survey and Research, 43(1), 63–71 (in Chinese with English abstract).

Gu AL, Wang J, Ren JP, Zuo LB, Sun HW, Wu XY, Xing S, Liu ZJ, Zhang JD, Chikambwe EM, Kasumba E. 2021. Petrogenesis of the Paleoproterozoic granitoids in Kapatu, northern Zambia: Constraints from geochemistry, zircon U-Pb chronology and Hf isotopes. Acta Geologica Sinica, 95(4), 999–1018 (in Chinese with English abstract). doi: 10.19762/j.cnki.dizhixuebao.2021030.

Kazimoto EO, Schenk V, Appel P. 2015. Granulite-facies metamorphic events in the northwestern Ubendian Belt of Tanzania: Implications for the Neoarchean to Paleoproterozoic crustal evolution. Precambrian Research, 256, 31–47. doi: 10.1016/j.precamres.2014.10.016.

Kabengele M, Lubala RT, Cabanis B. 1991. Caractérisation pétrologique et géochimique du magmatisme ubendien du secteur de Pepa-Lubumba, sur le plateau des Marungu (Nord-Est du Shaba, Zaire). Signification géodynamique dans l'évolution de la chaî ne ubendienne. Journal of African Earth Science, 13(2), 243–265.

Li HK, Geng JZ, Hao S, Zhang YQ, Li HM. 2009. Study on the determination of U-Pb isotopic age in zircons by laser ablation multicollector inductively coupled plasma mass spectrometry (LA-MC-ICPMS). Acta Mineralogica Sinica, 29(S1), 600–601 (in Chinese with English abstract). doi: 10.16461/j.cnki.1000-4734.2009.s1.014.

Liu YS, Gao S, Hu ZC, Gao CG, Zong KQ, Wang DB. 2010. Continental and oceanic crust recyclinginduced melt- peridotite interactions in the Trans- North China Orogen: U-Pb dating, Hf isotopes and trace elements in zircons from mantle xenoliths. Journal of Petrology, 51(1/2), 537–571.

Ludwig KR. 2003. User's manual for a geochronological toolkit for Microsoft Excel (Isoplot/Ex version 3. 0). Berkeley Geochronology Center Special Publication, 4, 1–76.

Lenoir JL, JP Liégeois, Theunissen K, Klerkx J. 1994. The Palaeoproterozoic Ubendian shear belt in Tanzania: geochronology and structure-ScienceDirect. Journal of African Earth Sciences, 19(3), 169–184. doi: 10.1016/0899-5362(94)90059-0.

Master S, Rainaud C, Armstrong RA, Phillips D, Robb LJ. 2005. Provenance ages of the Neoproterozoic Katanga Supergroup (Central African Copperbelt), with implications for basin evolution. Journal of African Earth Sciences, 42(1), 41–60.

Maniar PD, Piccoli PM. 1989. Tectonic discrimination of granitoids. Geological Society of America Bulletin, 101(5), 635–643. doi: 10.1130/0016-7606(1989)101<0635:TDOG>2.3.CO;2.

Möller A, Appel P, Mezger K, Schenk V. 1995. Evidence for a 2 Ga subduction zone: eclogites in the Usagaran Belt of Tanzania. Geology, 23(12), 1067–1070. doi: 10.1130/0091-7613(1995)023<1067:EFAGSZ>2.3.CO;2.

Pearce JA, Harris NBW, Tindle AG. 1984. Trace element discrimination diagrams for the tectonic interpretation of granitic rocks. Journal of Petrology, 25, 956–983. doi: 10.1093/petrology/25.4.956.

Rainaud CL, Armstrong RA, Master S, Robb LJ, Mumba PACC. 2002. Contributions to the geology and mineralisation of the central African copperbelt: I. Nature and geochronology of the pre-Katangan basement. In: Geological Survey of Namibia (Ed.), 11th IAGOD Quadrennial Symposium and Geocongress, Windhoek, Namibia, 5.

Rollinson HR. 1993. Using Geochemical Data: Evaluation, presentation, interpretation. New York, Longman Scientific and Technical, 1–352. doi: 10.1180/minmag.1994.058.392.25.

Rogers JJW, Santosh M. 2002. Configuration of Columbia, a Mesoproterozoic Supercontinent. Gondwanna Research, 5(1), 5–22. doi: 10.1016/S1342-937X(05)70883-2.

Ren JP, Wang J, Liu XY, He SF, He FQ, Xu KK. 2013. Research progresses on the Cu-Co deposits of Lufilian Area in the Mid-Southern Africa. Geological Science and Technology Information, 32(5), 142–152 (in Chinese with English abstract).

Ren JP, Zuo LB, Xu KK, Wang J, Liu XY, He SF, Liu Y, He FQ. 2016. Geodynamic evolution and mineral resources present research in Bangweulu Block, Northern Zambia. Geological Review, 4, 979–996 (in Chinese with English abstract). doi: 10.16509/j.georeview.2016.04.015.

Ren JP, Wang J, Gu AL, Zuo LB, Xu KK, Sun HW, Liu XY, He SF, He FQ. 2017a. Research status and prospecting potential of mineral resources in Lufilian Arc, Zambia. China Mining Magazine, 26(11), 139–144 (in Chinese with English abstract).

Ren JP, Wang J, Gu AL, Zuo LB, Sun HW, He FQ, Wang SY, Mukofu C, Dokowe AP, Chikambwe EM, Canisius C, Malunga D. 2018a. Detrital zircon fission track thermochronology in Kasama-Nondo, Northeastern Zambia. Atomic Energy Science and Technology, 52(12), 2275–2282 (in Chinese with English abstract). doi: 10.7538/yzk.2018.youxian.0252.

Ren JP, Wang J, Zhang DH, Dokowe AP, Chikambwe EM, Zuo LB, Xu KK, Liu XY, He FQ. 2018b. Reactivation of Lufilian Arc in Zambia: Zircon and apatite fission track chronology. Earth Science, 43(6), 1850–1860 (in Chinese with English abstract).

Ren JP, Wang J, Zuo LB, Gu AL, Sun HW, Xu KK, Mukofu C, Dokowe AP, Chikambwe E, Canisius C, Malunga D. 2019a. Zircon U-Pb geochronology, Lu-Hf isotopic compositions and geochemical characteristics of the quartz diorities from western Kasama in northern Zambia. Acta Geologica Sinica, 93(11), 2832–2846 (in Chinese with English abstract). doi: 10.19762/j.cnki.dizhixuebao.2019128.

Ren JP, Wang J, Gu AL, Sun HW, Xu KK, Wu XY. 2019b. U-Pb age and Lu-Hf isotopic characteristics of zircons from syenogranite in northeastern Zambia. Geological Survey and Research, 42(3), 161–165.

Ren JP, Wang J, Sun HW, Feng L, Zuo LB, Gu AL, He FQ, Mukofu C, Dokowe AP, Chikambwe EM, Canisius C, Malunga D. 2019c. Depositional environment of the Kasama Group, northeastern Zambia: Evidence from detrital zircon U-Pb-Hf isotopic compositions. Geology in China, 46(3), 575–586 (in Chinese with English abstract). doi: 10.12029/gc20190309.

Ren JP, Wang J, Zuo LB, Gu AL, Sun HW, Xu KK, He FQ, Mukofu C, Dokowe AP, Chikambwe EM, Cao SP, Cheng XJ. 2020. Enrichment characteristics of Cu and Co displayed by low-density geochemical mapping in Zambia. Journal of Geochemical Exploration, 219(2), 106634.

Ren JP, Wang J, Gu AL, Sun HW, Zuo LB, He FQ, Mukofu C, Dokowe AP, Chikambwe EM, Kasumba E. 2021a. Constraints of fission track dating after the Pan-African tectonic evolution of the Bangweulu Block, northeastern Zambia. Acta Geologica Sinica, 95(4), 1072–1081 (in Chinese with English abstract). doi: 10.19762/j.cnki.dizhixuebao.2021018.

Ren JP, Wang J, Gu AL, Zuo LB, Sun HW, Xu KK, He FQ, Mukofu C, Dokowe AP, Chikambwe EM, 2021b. Study on gold enrichment characteristics in Zambia: Based on 1∶1000000 geochemical mapping. China Geology. doi: 10.31035/cg2021034.

Schandelmeier H. 1980. Regionale Gliederung des Prkambriums and Aspeckte der Krustenentwicklung um Mambwe / Nordost-Zambia. Giessener Geologische Schrifttten 23. Lenz-Verlag, Giessen, 111.

Saviaro K. 1979. Preliminary analysis of airborne magnetic surveys in Zambia. In: G McEven (Editor), The Proceedings of a Seminar on Geophysics and the Exploration of the Kalahari. Bull. Geology Survey. Botswana, 22, 159–183.

Smit CA, VanReenen DD, Roering C. 2014. Role of fluids in the exhumation of the southern marginal zone of the Limpopo complex, South Africa. Precambrian Research, 253, 81–95. doi: 10.1016/j.precamres.2014.07.002.

Sun HW, Wang J, Ren JP, Gu AL, Zuo LB. 2019. Sedimentary stratigraphic characteristics of the Mporokoso Basin in the North-eastern Zambia. Geological Review, 65(1), 232–245 (in Chinese with English abstract). doi: 10.16509/j.georeview.2019.01.016.

Sun HW, Wang J, Ren JP, Gu AL, Zuo LB, Liu ZJ, Xing S, Su XY, Dokowe AP, Chikambwe EM. 2021. Study of U-Pb chronology and Hf isotopes of detrital zircons from metamorphic supracrustal rocks in the central part of the Bangweulu Block and its tectonic significance. Acta Geologica Sinica, 95(4), 1245–1259 (in Chinese with English abstract). doi: 10.19762/j.cnki.dizhixuebao.2021019.

Sylvester PJ. 1998. Post-collisional strongly peraluminous granites. Lithos, 45(1/4), 29–44.

Sun SS, McDonough WF. 1989. Chemical and isotopic systematics of oceanic basalts: Implications of mantle composition and processes. In: Saunders AD and Norry MJ (Eds.). Magmatism in the Ocean Basins. Geological Society of London, Special Publication, 42, 313–345.

Sun K, Zhang LL, Zhao ZD, He FQ, He SF, Wu XY, Qiu L, Ren XD. 2018. Episodic crustal growth in the Tanzania Craton: Evidence from Nd isotope compositions. China Geology, 1, 210–224. doi: 10.31035/cg2018025.

Taylor SR, McLennan SM. 1985. The continental crust: Its composition and evolution. Oxford, UK, Blackwell Scientific Publications, 1–312.

Wu YB, Zheng YF. 2004. Zircon genetic mineralogy and its constraints on U-Pb age interpretation. Chinese Science Bulletin, 49(16), 1589–1604 (in Chinese with English abstract). doi: 10.1360/csb2004-49-16-1589.

Whalen JB, Currie KL, Chappell BW. 1987. A-type granites: Geochemical characteristics, discrimination and petrogenesis. Contributions to Mineralogy and Petrology, 95(4), 407–419. doi: 10.1007/BF00402202.

White AKR, Chappell BW. 1977. Ultrametamorphism and granitoid genesis. Tectonophysics, 43, 7–22. doi: 10.1016/0040-1951(77)90003-8.

Xing S, Ji SQ, Wang J, Ren JP, Liu ZJ, Gu AL, Sun HW, Zhang JD, Liu C, Zhang DL. 2021. Detrital zircon U-Pb dating and Hf isotope analyses of the Kabwelumu Formation, northeastern Zambia. Acta Geologica Sinica, 95(4), 1191–1211 (in Chinese with English abstract). doi: 10.19762/j.cnki.dizhixuebao.2021023.

Zhao GC, Cawood PA, Wilde SA, Sun M. 2002. Review of global 2. 1 –1. 8 Ga orogens:Implications for a Pre-Rodinia Supercontinent. Earth Science Reviews, 59, 125–162.

Zhai MG. 2010. Tectonic evolution and metallogenesis of North China Craton. Mineral Deposits, 29(1), 24–36 (in Chinese with English abstract). doi: 10.16111/j.0258-7106.2010.01.006.

Zhou TF, Yuan F, Zhang DY, Fan Y, Liu S, Peng MX, Zhang JD. 2010. Geochronology, tectonic setting and mineralization of granitoids in Jueluotage area, eastern Tianshan, Xinjiang. Acta Petrologica Sinica, 26(2), 478–502 (in Chinese with English abstract).

Zuo LB, Ren JP, Wang J, Gu AL, Sun HW, Xu KK. 2020. Geochemical characteristics, Zircon U-Pb ages and Lu-Hf isotopic composition of granites in Bangweulu Block, Zambia. Geological Survey and Research, 43(1), 30–41 (in Chinese with English abstract).

Zuo LB, Ren JP, Qiu L, Wang J, Gu AL, Sun HW, Xu KK, Dokowe AP, Mukangwa A, Malunga D, Mwansa C, Chipumbu P. 2021. Zircon U-Pb geochronology, geochemical characteristics and petrogenesis of the gneisses in the eastern Isoka, Zambia. Acta Geologica Sinica, 95(4), 1144–1158 (in Chinese with English abstract). doi: 10.19762/j.cnki.dizhixuebao.2021037.